Numerical Instability Curing of Roe's Flux-Difference Splitting by Modified *H*-Correction Entropy Fix on Unstructured Meshes

Sutthisak PHONGTHANAPANICH and Pramote DECHAUMPHAI

Department of Mechanical Engineering, Faculty of Engineering,

Chulalongkorn University 10330, Thailand

Tel: 0-2218-6621 Fax: 0-2218-6621 E-mail: fmepdc@eng.chula.ac.th

Abstract

This paper presents a study of numerical instability for the Roe's FDS on triangular meshes. The *H*-correction entropy fix is modified and included in the upwinding algorithm for unstructured triangular meshes to improve the computed shock wave resolution. The solution accuracy is further improved by coupling an error estimation procedure with an adaptive remeshing algorithm. Efficiency of the combined procedure is evaluated by analyzing supersonic shocks and shock propagation behaviors for both the steady and unsteady high-speed compressible flows.

1. Introduction

High-speed compressible flows normally involve complex flow phenomena, such as strong shock waves, shock-shock interactions and shear layers. Various numerical inviscid flux formulations have been proposed to solve an approximate Riemann problem. Among these formulations, the flux-difference splitting scheme by Roe [1] is widely used due to its accuracy, quality and mathematical clarity. However, the scheme may sometimes lead to unphysical flow solutions in certain problems. As an example of the odd-even decoupling problem [2], an unrealistic perturbation may grow with the planar shock as it moves along the duct.

The main objectives of this paper are to propose and evaluate a modified Roe's scheme on adaptive unstructured meshes for two-dimensional high-speed compressible flow analysis. The *H*-correction entropy fix [3] is modified for unstructured triangular meshes and implemented into the original Roe's scheme. To improve the analysis solution accuracy, the presented scheme is further extended to high-order solution accuracy and combined with an adaptive remeshing procedure. The efficiency of the combined procedure is evaluated by analyzing a series of both steady and unsteady high-speed compressible flows.

2. Numerical technique

The finite volume formulation of two-dimensional Euler equations for high-speed compressible flows of an element with domain Ω may be written in the form,

$$\frac{\partial}{\partial t}\int_{\Omega}\vec{U}\,d\Omega+\oint_{\partial\Omega}\vec{F}\cdot\vec{n}dS=0 \tag{1}$$

where Ω is a control volume. $\vec{U}$ is the vector of conservative variables, and $\vec{F}$ is the vector of the convective fluxes. The Roe's approximate Riemann solver (**Roe**) is implemented in the framework of the cell-centered scheme. The numerical flux, passing through a shared side of the two adjacent left and right elements is given by [1],

$$\boldsymbol{F}_n=\frac{1}{2}(\boldsymbol{F}_{nL}+\boldsymbol{F}_{nR})-\frac{1}{2}\sum_{k=1}^{4}\alpha_k\left|\lambda_k\right|\boldsymbol{r}_k \tag{2}$$

where α_k is the wave strength of the k^{th} wave, λ_k is the eigenvalue in $\lfloor V_n-a \quad V_n \quad V_n \quad V_n+a\rfloor^T$, V_n is the normal velocity, a is the speed of sound at the cell interface, and $\boldsymbol{r}_k$ is the corresponding right eigenvector.

Sanders *et al*. [3] introduced an idea of a multidimensional dissipation, the so called *H*-correction entropy fix method. The method has shown to eliminate the unrealistic carbuncle phenomenon of the flow over a blunt body in the structured uniform mesh as shown in Fig. 1(a). The advantages of the method are the simplicity in the implementation into the existing scheme and the parameter-free characteristics. For the two triangular cells shown in Fig. 1(b), the *H*-correction entropy fix according to Sanders *et al.*, (**RoeSA**) has been modified to [4],

$$\eta^{SA} = \max(\eta_1, \eta_2, \eta_3, \eta_4, \eta_5) \qquad (3)$$

where η_i, i = 1 to 5 are,

$$\eta_i = 0.5 \max_k (|\lambda_{kR} - \lambda_{kL}|) \qquad (4)$$

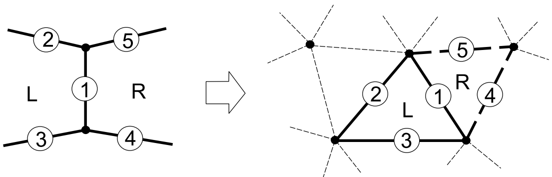

(a) (b)

Fig. 1. Cell interfaces of: (a) structured uniform mesh; (b) unstructured triangular mesh.

Then the eigenvalues are modified according to Ref. [5] yielding,

$$\lambda_k^{SA} = \max\left(\lambda_k, \eta^{SA}\right) \qquad (5)$$

The above method has been evaluated using three test cases of expansion shocks, an odd-even decoupling, and a kinked Mach stem, as presented in the following sections.

3. Algorithm evaluation

To illustrate an unphysical expansion shock, a Mach 3 flow over a forward facing step [6] is investigated. The density contours computed from the **Roe** and **RoeSA**, are shown in Fig. 2(a)-(b), respectively. The figures show that the **Roe** produces an unphysical expansion shock on top of the facing step corner, whereas the **RoeSA** provides realistic solution.

The next test case is a Mach 6 moving shock along odd-even grid perturbation in a straight duct [2]. The computational domain consists of a uniform triangular mesh with 800 and 20 equal intervals, respectively, along the axial and the transverse directions of the duct. The grids along the duct centerline are perturbed in the transverse direction with the magnitude of $\pm 10^{-6}$. The **RoeSA** can provide accurate shock resolution whereas the **Roe** suffers from the numerical instabilities as depicted in Figs. 3(a)-(h), respectively. As explained by Gressier and Moschetta [7], the exact capture of contact discontinuity and strict stability cannot be simultaneously satisfied in any upwind scheme. The solution suggests that additional dissipation injection to the entropy and shear waves is thus needed to stabilize the Roe's scheme as done by **RoeSA**.

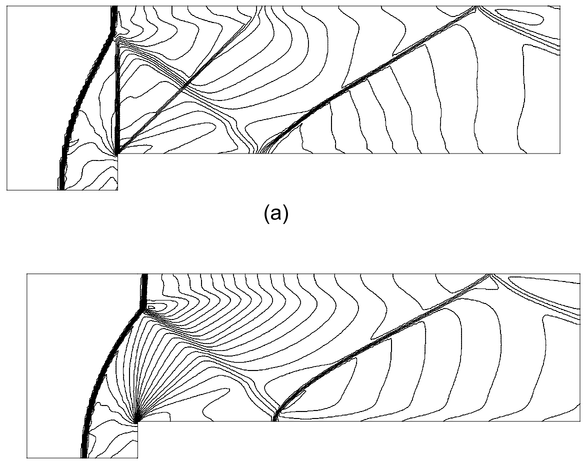

(a)

(b)

Fig. 2. A Mach 3 flow over a forward facing step: (a) **Roe**; and (b) **RoeSA**.

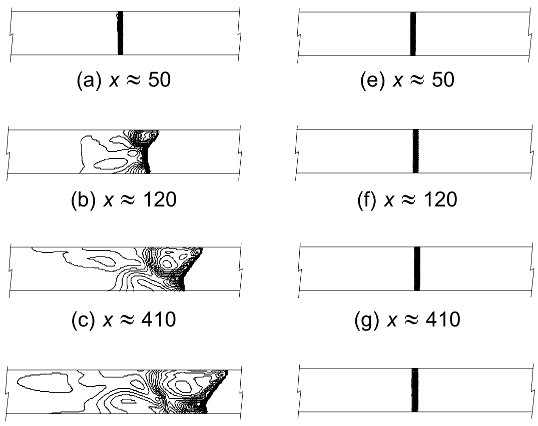

(a) $x \approx 50$ (e) $x \approx 50$

(b) $x \approx 120$ (f) $x \approx 120$

(c) $x \approx 410$ (g) $x \approx 410$

(d) $x \approx 610$ (h) $x \approx 610$

Fig. 3. A Mach 6 moving shock along odd-even grid perturbation: (a)-(d) **Roe**; and (e)-(h) **RoeSA.**

A kinked Mach stem generated from a shock moving over a ramp is the last test case used to highlight the performance of this method. Figures 4(a)-(b) respectively show the density contours obtained from the **Roe** and **RoeSA** for a Mach 5 normal shock moving over a 46^{o} ramp. The **RoeSA** provides reasonable accurate solutions such that the kinked Mach stem is recovered with the slightly broken-down incident shock. The **Roe**, however, yields the broken-down incident shock with severely kinked mach stem. Such solution may be caused by insufficient dissipation that cannot counteract the transverse perturbation [2,7].

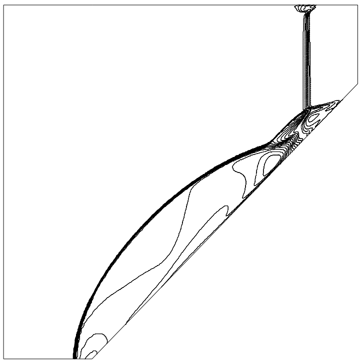

(a)

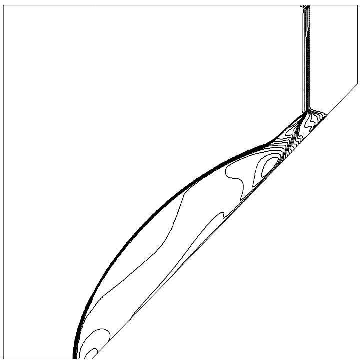

(b)

Fig. 4. A kinked Mach stem from a Mach 5 shock moving over a 46° ramp: (a) **Roe**; and (b) **RoeSA**.

4. High-order extension and applications on triangular meshes

Solution accuracy from the first-order formulation described in the preceding sections can be improved by implementing a high-order formulation for both the space and time. A high-order spatial discretization is achieved by applying the Taylor' series expansion to the cell-centered solution for each cell face [8]. For instance, the solutions at the midpoint of an element edge between node 1 and 2 shown in Fig. 5, can be reconstructed from,

$$\boldsymbol{q}_{f_{1-2}} = \boldsymbol{q}_C + \frac{\Psi_C}{3}\left[\frac{(\boldsymbol{q}_1+\boldsymbol{q}_2)}{2} - \boldsymbol{q}_3\right] \tag{6}$$

where $\boldsymbol{q} = [\rho \quad u \quad v \quad p]^T$ consists the primitive variables of the density, the velocity components, and the pressure, respectively; $\boldsymbol{q}_C$ is the solution at the element centroid; $\boldsymbol{q}_n$, n = 1, 2, 3 are the solutions at nodes. In this paper, the inverse-distance weighting from the centroid to the nodes that preserves the principle of positivity [9] is used,

$$\boldsymbol{q}_n = \sum_{i=1}^{N}\frac{\boldsymbol{q}_{C,i}}{|\vec{\boldsymbol{r}}_i|}\Bigg/\sum_{i=1}^{N}\frac{1}{|\vec{\boldsymbol{r}}_i|} \tag{7}$$

where $\boldsymbol{q}_{C,i}$ are the surrounding cell-centered values of node n. $|\vec{\boldsymbol{r}}_i|$ is the distance from the centroid to node n, and N is the number of the surrounding cells.

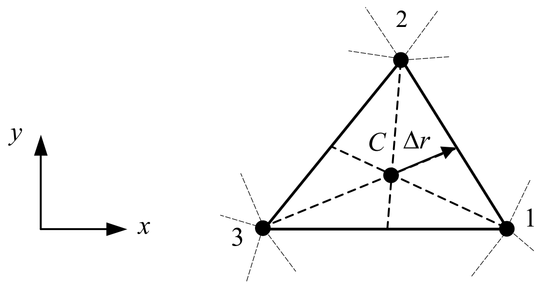

Fig. 5. Linear reconstruction on a typical triangular element.

The Ψ_C in Eq. (6) represents the limiter for preventing spurious oscillation that may occur in the region of high gradients. In this study, the Vekatakrishnan's limiter function [10] is selected,

$$\Psi_C = \min_{i=1,2,3}\begin{cases}\phi\left(\dfrac{\Delta_{+,\max}}{\Delta_-}\right) & , \Delta_- \geq 0 \\ \phi\left(\dfrac{\Delta_{+,\min}}{\Delta_-}\right) & , \Delta_- < 0 \\ 1 & , \Delta_- = 0\end{cases} \tag{8}$$

where $\Delta_- = \boldsymbol{q}_c - \boldsymbol{q}_i$, $\Delta_{+,\max} = \boldsymbol{q}_{\max} - \boldsymbol{q}_i$, and $\Delta_{+,\min} = \boldsymbol{q}_{\min} - \boldsymbol{q}_i$. The $\boldsymbol{q}_{\max}$ and $\boldsymbol{q}_{\min}$ are respectively the maximum and minimum values of all distance-one neighboring cells. The function ϕ is similar to the Van Albada limiter [11], which is expressed in the form,

$$\phi(y) = \frac{y^2+2y}{y^2+y+2} \tag{9}$$

The second-order temporal accuracy is achieved by implementing the second-order accurate Runge-Kutta time stepping method [12],

$$\begin{aligned} \boldsymbol{U}_i^* &= \boldsymbol{U}_i^n - \frac{\Delta t}{\Omega_i}\sum_{j=1}^{3}\boldsymbol{F}^n \cdot \boldsymbol{n}_j \\ \boldsymbol{U}_i^{n+1} &= \frac{1}{2}\left[\boldsymbol{U}_i^0 + \boldsymbol{U}_i^* - \frac{\Delta t}{\Omega_i}\sum_{j=1}^{3}\boldsymbol{F}^* \cdot \boldsymbol{n}_j\right] \end{aligned} \tag{10}$$

where Δt is the time step. Local element time steps are used for steady-state analysis, while the minimum global time step based on spectral radii [13] is used for the unsteady analysis to reduce the computation effort.

The high-order extension of the Roe's scheme with the mixed entropy fix method, **RoeSA,** presented in the preceding section is evaluated by solving test cases. The modified scheme is also combined with an adaptive meshing technique that generates unstructured triangular meshes for more complex problems. The selected test cases are: (1) Sod shock tube, (2) Supersonic flow over a bump, and (3) Steady-state Mach 15.3 flow past a cylinder.

Sod shock tube – The one-dimensional shock tube test case, the so called Sod shock tube [14], is solved by using a two-dimensional domain. The initial conditions of the fluids on the left and right sides are given by $(\rho, u, p)_L$ = (1.0, 0.0, 1.0) and $(\rho, u, p)_R$ = (0.125, 0.0, 0.1). The 1.0 x 0.1 computational domain is discretized with uniform triangular elements into 200 and 20 equal intervals in the *x* and *y* directions, respectively. Figures 6(a)-(b) show the predicted density and pressure for both first and second-order accurate distributions along the tube length and are compared with the exact solutions at time *t* = 0.15. The figures show that the second-order extension of Roe's scheme with the entropy fix **RoeSA** provides more accurate solutions.

Supersonic flow over a bump – The second-order **RoeSA** is further evaluated for adaptive unstructured meshes using a problem with more complex flow phenomena. Figure 7 shows the problem statement of a supersonic Mach 1.4 flow over a 4% bump [15] which results in more complex flow behavior. The initial mesh and the corresponding density contours computed by using the second-order **RoeSA** are shown in Figs. 8(a)-(b), respectively. The adaptive meshing technique is then used to capture solution discontinuities in order to enhance the solution accuracy. The final adaptive mesh and the corresponding density contours computed by using the second-order **RoeSA** are shown in Figs. 9(a)-(b), respectively. The figures highlight the use of the second-order accurate scheme on adaptive meshes to effectively obtain detailed flow solution.

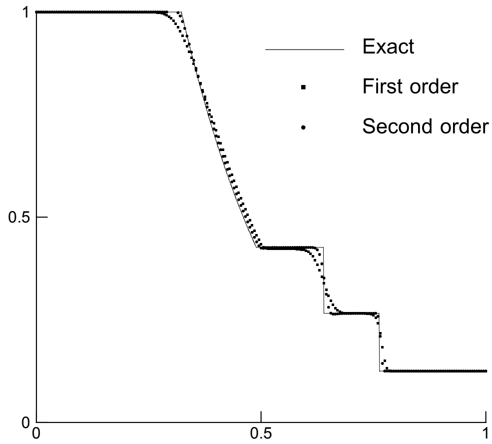

(a)

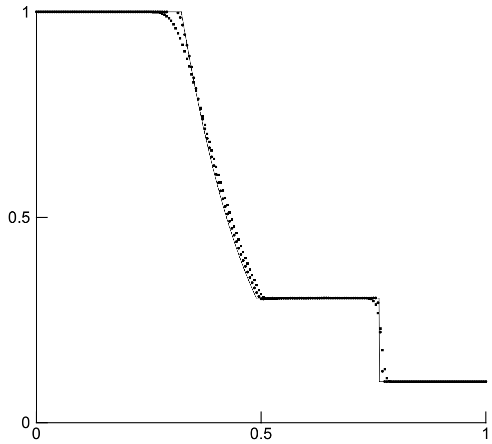

(b)

Fig. 6. Comparative predicted and exact solutions at time *t* = 0.15 for Sod shock tube (**RoeSA**): (a) Density distributions; and (b) Pressure distributions.

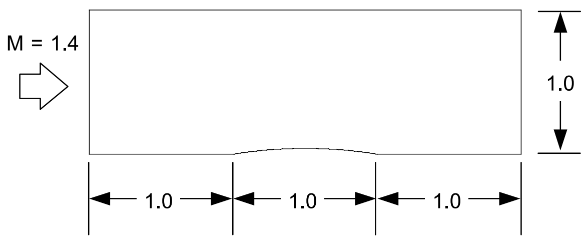

Fig. 7. Problem statement of a supersonic flow over a bump.

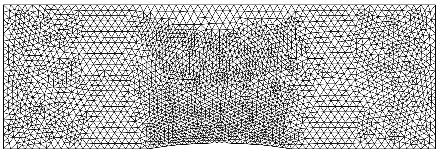

(a)

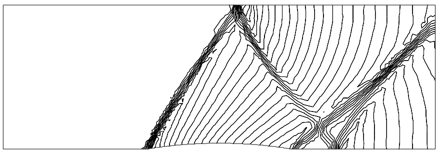

(b)

Fig. 8. A Mach 1.4 flow over a bump (**RoeSA**): (a) Initial mesh; and (b) Corresponding density contours.

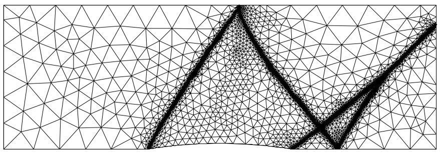

(a)

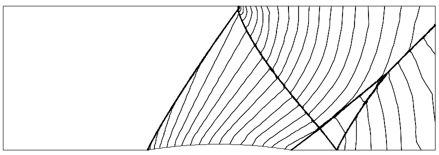

(b)

Fig. 9. A Mach 1.4 flow over a bump (**RoeSA**): (a) Final mesh; and (b) Corresponding density contours.

Steady-state Mach 15.3 flow past a cylinder – A steady-state Mach 15.3 flow past a cylinder [4] described in Fig. 10 is used to demonstrate the solution accuracy improvement by coupling the **RoeSA** and the adaptive meshing algorithm. Figures 11(a)-(d) show the final adaptive mesh consisting of 36,986 elements, with the resulting density, pressure and Mach number contours.

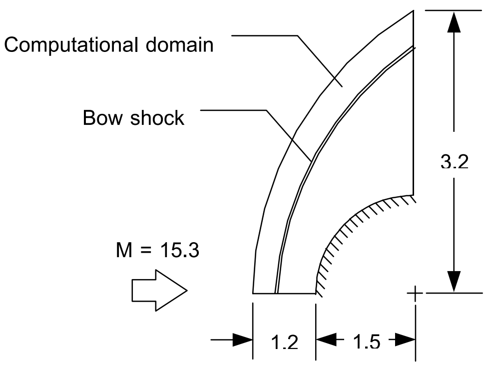

Fig. 10. Problem statement of a Mach 15.3 flow past a cylinder.

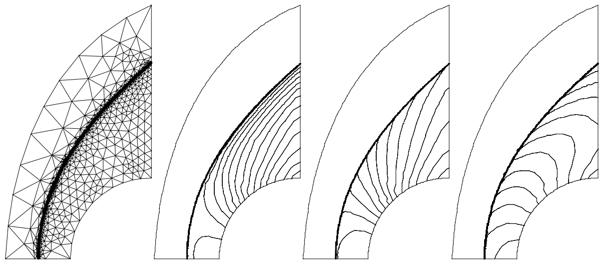

(a) (b) (c) (d)

Fig. 11. A Mach 15.3 flow past a cylinder: (a) Adaptive mesh; (b) Density contours; (c) Pressure contours; and (d) Mach number contours.

5. Conclusion

The modified *H*-correction entropy fix for triangular meshes is proposed to improve numerical stability of the Roe's flux-difference splitting scheme. The method was evaluated by several well-known test cases and found to eliminate unphysical solutions that may arise from the use of the original Roe's scheme. These unphysical solutions include the expansion shock generated from the flow over a forward facing step and the numerical instability from the odd-even decoupling problem. To further improve solution accuracy, the second-order spatial and second-order Runge-Kutta temporal discretization were also implemented. The method was also combined with an adaptive mesh generation technique to demonstrate its applicability for arbitrary unstructured meshes. The entire process was found to provide more accurate solutions for both the steady-state and transient flow test cases.

Acknowledgement

The authors are pleased to acknowledge the Thailand Research Fund (TRF) for supporting this research work.

References

[1] Roe, P. L. "Approximate Riemann Solvers, Parameter Vectors, and Difference Schemes", Journal of Computational Physics, 1981, Vol. 43, pp. 357-372.

[2] Quirk, J. J. "A Contribution to the Great Riemann Solver Debate", International Journal for Numerical Methods in Fluids, 1994, Vol. 18, pp. 555-574.

[3] Sanders, R., Morano, E., and Druguet M.C. "Multidimensional Dissipation for Upwind Schemes: Stability and Applications to Gas Dynamics", Journal of Computational Physics, 1998, Vol. 145, pp. 511-537.

[4] Dechaumphai, P. and Phongthanapanich, S., "High-Speed Compressible Flow Solutions by Adaptive Cell-Centered Upwinding Algorithm with Modified *H*-Correction Entropy Fix", Advances in Engineering Software, 2003, Vol. 34, pp. 533-538.

[5] Harten, A. "High Resolution Schemes for Hyperbolic Conservation Laws", Journal of Computational Physics, 1983, Vol. 49, pp. 357-393.

[6] Woodward, P. and Colella, P. "The Numerical Simulation of Two-Dimensional Fluid Flow with Strong Shocks", Journal of Computational Physics, 1984, Vol. 54, pp. 115-173.

[7] Gressier, J. and Moschetta, J. M. "Robustness versus Accuracy in Shock-Wave Computations", International Journal for Numerical Methods in Fluids, 2000, Vol. 33, pp. 313-332.

[8] Frink, N. T., Parikh, P. and Pirzadeh, S. "A Fast Upwind Solver for the Euler Equations on Three-Dimensional Unstructured Meshes", AIAA Paper-91-0102, Nevada, 1991.

[9] Frink, N. T. and Pirzadeh, S. Z. "Tetrahedral Finite-Volume Solutions to the Navier-Stokes Equations on Complex Configurations", NASA/TM-1998-208961, 1998.

[10] Vekatakrishnan, V. "Convergence to Steady State Solutions of the Euler Equations on Unstructured Grids with Limiters", Journal of Computational Physics, 1995, Vol. 118, pp. 120-130.

[11] Van Albada, G. D., Van Leer, B. and Roberts, W. W. "A Comparative Study of Computational Methods in Cosmic Gas Dynamics", Astronomy and Astrophysics, 1982, Vol. 108, pp. 76-84.

[12] Shu, C. W. and Osher, S. "Efficient Implementation of Essentially Non-Oscillatory Shock-Capturing Schemes", Journal of Computational Physics, 1988, Vol. 77, pp. 439-471.

[13] Vijayan, P. and Kallinderis, Y. "A 3D Finite-Volume Scheme for the Euler Equations on Adaptive Tetrahedral Grids", Journal of Computational Physics, 1994, Vol. 113, pp. 249-267.

[14] Sod, G. A. "A Survey of Several Finite Difference Methods for Systems of Nonlinear Hyperbolic Conservation Laws", Journal of Computational Physics, 1978, Vol. 27, pp. 1-31.

[15] Hendriana, D. and Bathe, K. J. "On a Parabolic Quadrilateral Finite Element for Compressible Flows", Computer Methods in Applied Mechanics and Engineering, 2000, Vol. 186, pp. 1-22.